Measurement of the soft polariton in $KTa_{0.93}Nb_{0.07}O_3$ by time-resolved four-wave mixing

P. Grenier
Département de Physique, Université de Sherbrooke, Sherbrooke, Québec, Canada J1K 2R1

D. Houde
Département de Médecine Nucléaire et de Radiobiologie, Université de Sherbrooke, Sherbrooke, Québec, Canada J1K 2R1

S. Jandl
Département de Physique, Université de Sherbrooke, Sherbrooke, Québec, Canada J1K 2R1

L. A. Boatner
Solid State Division, Oak Ridge National Laboratory, P.O. Box 2008, Oak Ridge, Tennessee 37831-6056
(Received 23 February 1994; revised manuscript received 25 July 1994)

Measurement of the A_1(TO) soft-polariton mode in $KTa_{0.93}Nb_{0.07}O_3$ has been made as a function of wave vector and temperature by means of a time-resolved third-order optical susceptibility technique. With the use of a polariton model calculation, the A_1(TO) soft-phonon mode self-energy wave-vector dependence, the Raman tensor, and the electro-optic tensor are inferred. The results indicate the particularity of the soft-phonon mode dynamics in the polariton region. The soft-phonon self-energy shows the presence of a four-particule interaction relaxation process and of an additional relaxation process associated with the intercluster dynamics, while the Raman and electro-optic tensor behavior as a function of temperature indicates the predominance of the electromagnetic interaction in the soft-phonon mode dynamics close to T_c.

I. INTRODUCTION

Recently, the results of a number of impulsive-stimulated-scattering (ISS) experiments on perovskites have been reported.[1–9] Renewed interest in the perovskites is, in fact, attributable in part to the ability of this experimental technique to provide new information regarding the dynamical behavior of such systems.

The dynamical behavior associated with structural phase transitions in perovskite-structure materials is a subject of long-standing research interest and activity.[10–12] In particular, the relationship between the "relaxation-mode" versus "soft-mode" dynamics and the relative importance of "order-disorder" versus "displacive" effects in driving the phase transition remain subjects of current controversy.[7,13–15]

An ISS experiment is advantageous, as compared to a Raman scattering experiment, in two ways: First, vibrational oscillations and decays, associated respectively with the soft mode and Debye-relaxation mode, give rise to different contributions in an ISS time domain experiment contrary to a spectral-domain experiment where these contributions are equivalent. The relative merits of the two experimental approaches have been compared in both theoretical and practical terms.[6,7,16,17] Second, ISS experiments are usually performed at small scattering angles to maximize the overlap of the crossed laser pulses. Therefore, a polariton dispersion measurement is a common feature of an ISS experiment on polar phonons, while it is a difficult task in a Raman scattering experiment. Investigations of the polariton dispersion relation are helpful in understanding phase transitions in perovskites since they give information on the soft-phonon mode (e.g., its self-energy as a function of frequency and wave vector) and permit an evaluation of the static dielectric constant.[1,2,5,9]

The present work represents an in-depth study of the A_1 polariton-dispersion relation in $KTa_{0.93}Nb_{0.07}O_3$ as a function of temperature by the ISS technique. In Sec. II we present the theory of the ISS experiment involving a phonon-polariton mode and describe how to relate the polariton characteristics to those of the phonons. Hence, the polariton propagators are calculated, in Appendix A, by the diagonalization of the phonon-photon Hamiltonian, and the polariton lifetime is introduced through the third-order phonon-phonon interaction mechanical anharmonicity. Then a generalization of the formalism used to describe the ISS experiment with these propagators is given in Appendix B. This allows one to deduce the phonon self-energy wave-vector dependence, the Raman tensor, and the electro-optic tensor from the experimental data. Section III describes the experimental setup, while the results are presented and analyzed in Sec. IV. These findings in relation to the phase transition are discussed in Sec. V.

II. THEORETICAL BACKGROUND

Extensive discussions of ISS experiments in the general case have been presented by Yan-Nelson,[16,17] and in

 ©1994 The American Physical Society

the particular case of scattering by a polariton mode, by Dougherty *et al.*[5] Here we will use the same formalism as that of Ref. 16, differing only in the way we describe the polariton mode. A detailed calculation of the polariton mode is carried out in Appendix A and is included within the Yan-Nelson formalism in Appendix B. The main result is Eq. (B8) which gives the impulse-response function associated with the polariton mode. As discussed in a previous paper,[3] in order to account for the instantaneous part of the response and to obtain the total response function, a Dirac function $\delta(t)$ is added. Consequently, the diffraction efficiency as a function of time delay τ_d between the pump and probe pulse, at a given wave-vector transfer (k), can be expressed as

$$S(\tau_d) = \int dt \left\{ \int d\tau \left[A\delta(\tau) + \frac{f_\rho(k)}{\Omega_{k\rho}} \exp(-\gamma_{k\rho}\tau) \sin[\Omega_{k\rho}\tau + \varphi_\rho(k)] \right] I_p(t-\tau) \right\}^2 I_t(t-\tau_d) \ , \tag{2.1}$$

where A is the amplitude associated with the instantaneous part of the response. $\Omega_{k\rho}$ and $\gamma_{k\rho}$ are the real and imaginary parts of the branch ρ polariton propagator poles ($\tilde{\omega}_{k\rho} = \pm\Omega_{k\rho} - i\gamma_{k\rho}$). $I_p(t)$ and $I_t(t)$ represent the pump- and probe-pulse profiles, respectively. An analysis of the polariton-response-function amplitude $[f_\rho(k)]$ and phase $[\varphi_\rho(k)]$ dependence on the wave vector and on the relative contribution of the Raman tensor and electro-optic tensor is given in Appendix B.

Through Eq. (2.1), the experimental results provide access to the polariton frequency $(\Omega_{k\rho})$ and damping rate $(\gamma_{k\rho})$. Using Eq. (A17), the phonon self-energy $[\Sigma(\mathbf{k},\omega) = \Sigma^R(\mathbf{k},\omega) + 2i\omega\Sigma^I(\mathbf{k},\omega)]$ at the polariton poles $(\omega = \tilde{\omega}_{k\rho})$ is inferred. According to standard many-particle-system perturbation theory,[18,19] the self-energy gives the frequency and the damping rate renormalizations brought about by the anharmonic interactions.

In our case, where the ionic plasma frequency is much greater than the transverse phonon frequency $(\Omega_p \gg \omega_{\mathrm{TO}})$, we obtain for the lower polariton branch $(\rho = 1)$

$$\Sigma^I(\mathbf{k}, \omega = \tilde{\omega}_{k1}) \simeq \frac{(ck/n)^2 + \Omega_p^2}{(ck/n)^2} \gamma_{k1} \ , \tag{2.2a}$$

$$\Sigma^R(\mathbf{k}, \omega = \tilde{\omega}_{k1}) \simeq \omega_{\mathrm{TO}}^2 - \frac{(ck/n)^2 + \Omega_p^2}{(ck/n)^2} \left[\Omega_{k1}^2 + \gamma_{k1}^2\right] \ . \tag{2.2b}$$

Note that ω_{TO} does not influence $\Sigma^I(\mathbf{k},\omega)$ and only adds a constant value to $\Sigma^R(\mathbf{k},\omega)$.

III. EXPERIMENTAL SETUP

The present investigation was carried out using a single crystal of $KTa_{0.93}Nb_{0.07}O_3$ with a transition temperature T_c of $\sim$ 68 K. This crystal, whose dimensions are $0.25 \times 1.6 \times 5.0$ mm^3, was cut along the rhombohedral axes ($a = [2\bar{1}\bar{1}]$, $b = [01\bar{1}]$, $c = [111]$). An electric field of $\sim$3.0 kV/cm was applied along the c axis during the cooling process in order to pole the sample. When the sample temperature was stabilized at 15 K, the field was decreased to 600 V/cm, and the experiment was then performed with this residual field. The maintenance of this residual field is required during the measurements since the domains produced by cooling in the 3.0 kV/cm field tend to relax even at temperatures as low as $T = 10$ K. This relaxation results in a decrease in the diffracted signal and an accompanying increase in the scattering of the pump pulses.

The experiment was performed using a forward-folded boxcar geometry[20] with two pump pulses at 620 nm and a probe pulse at 650 nm. Both the pump and probe pulses have a temporal width of $\sim$ 100 fs. The two pump pulses make an angle $\theta \in [0.6°, 3.57°]$ inside the crystal. The wave-vector transfer $(\mathbf{k})$ is then

$$|\mathbf{k}|^2 = |\mathbf{k}_{p1}|^2 + |\mathbf{k}_{p2}|^2 - 2|\mathbf{k}_{p1}||\mathbf{k}_{p2}|\cos\theta \ , \tag{3.1}$$

where $\mathbf{k}_{p1,2}$ represents the pump wave vectors. The frequency (Ω_{k1}) of the generated mode being small we can neglect the refractive index (n) dispersion and obtain

$$\frac{ck}{n} = \left[\left(\omega_0 + \frac{\Omega_{k1}}{2}\right)^2 + \left(\omega_0 - \frac{\Omega_{k1}}{2}\right)^2 - 2\left(\omega_0 + \frac{\Omega_{k1}}{2}\right)\left(\omega_0 - \frac{\Omega_{k1}}{2}\right)\cos\theta \right]^{1/2} \ , \tag{3.2}$$

where ω_0 is the central pump frequency. The pump pulses are incident along the direction of the a axis and are polarized along the c axis. The resulting polaritons propagate along the b axis and are of A_1 symmetry. The diffracted signal, which is polarized along the c axis, permits the measurement of the $\chi^{(3)}_{cccc}$ susceptibility-tensor element.

IV. EXPERIMENTAL RESULTS

The observed diffraction efficiency of $KTa_{0.93}Nb_{0.07}O_3$ as a function of the probe-pulse time delay for several wave-vector transfers and of temperature below T_c is illustrated in Figs. 1(a)–1(f). The frequency Ω_{k1} and the damping γ_{k1} obtained from a least-squares fit to the data using Eq. (2.1) are illustrated in Figs. 2(a)–2(f). While experimental data were obtained for 10 K $\leq T \leq$ 62 K, no precise determination of the frequency and the damping could be made for $T > 53$ K. The instantaneous and the polariton contributions to the diffraction efficiency have been plotted separately on curves $T = 10$ K and $T = 50$ K of Fig. 1(d). They correspond to the dotted and dashed lines, respectively. From the diffraction efficiency at $T = 50$ K, it is clearly seen that the instantaneous and the polariton responses contribute almost equally to the diffraction efficiency peak around zero time delay. Nevertheless, the absence of oscillations in the polariton response, due to the high damping rate, makes it difficult to determine the associated frequency and damping. For the same reason, the phase $\varphi_1(k)$ in Eq. (2.1) could be

determined only at very low temperatures where some oscillations are seen. Its value is smaller than $\varphi_1(k) < 15°$, and no particular wave-vector dependence was observed. The solid curve in Fig. 2(a) is a least-squares fit to the data using Eq. (A17) in the case of a constant damping rate for the phonon self-energy [i.e., $\Sigma^R(\mathbf{k},\omega) = 0$ and $\Sigma^I(\mathbf{k},\omega) = \gamma_{TO}$]. Values obtained for the parameters are $\Omega_p = 771 \pm 73$ cm^{-1}, $\omega_{TO} = 82 \pm 3$ cm^{-1}, and $\gamma_{TO} = 13 \pm 2$ cm^{-1}. These values, except for γ_{TO}, agree with the results of Raman and infrared reflectivity experiments.[21]

From the experimental values of the frequencies and damping rates, and using Eq. (A17), we can deduce the phonon self-energy as a function of wave vector and temperature. This is presented in Figs. 3(a)–3(c) and Figs. 4(a)–4(c) where $\Sigma(\mathbf{k},\omega)$ values are plotted, for con-

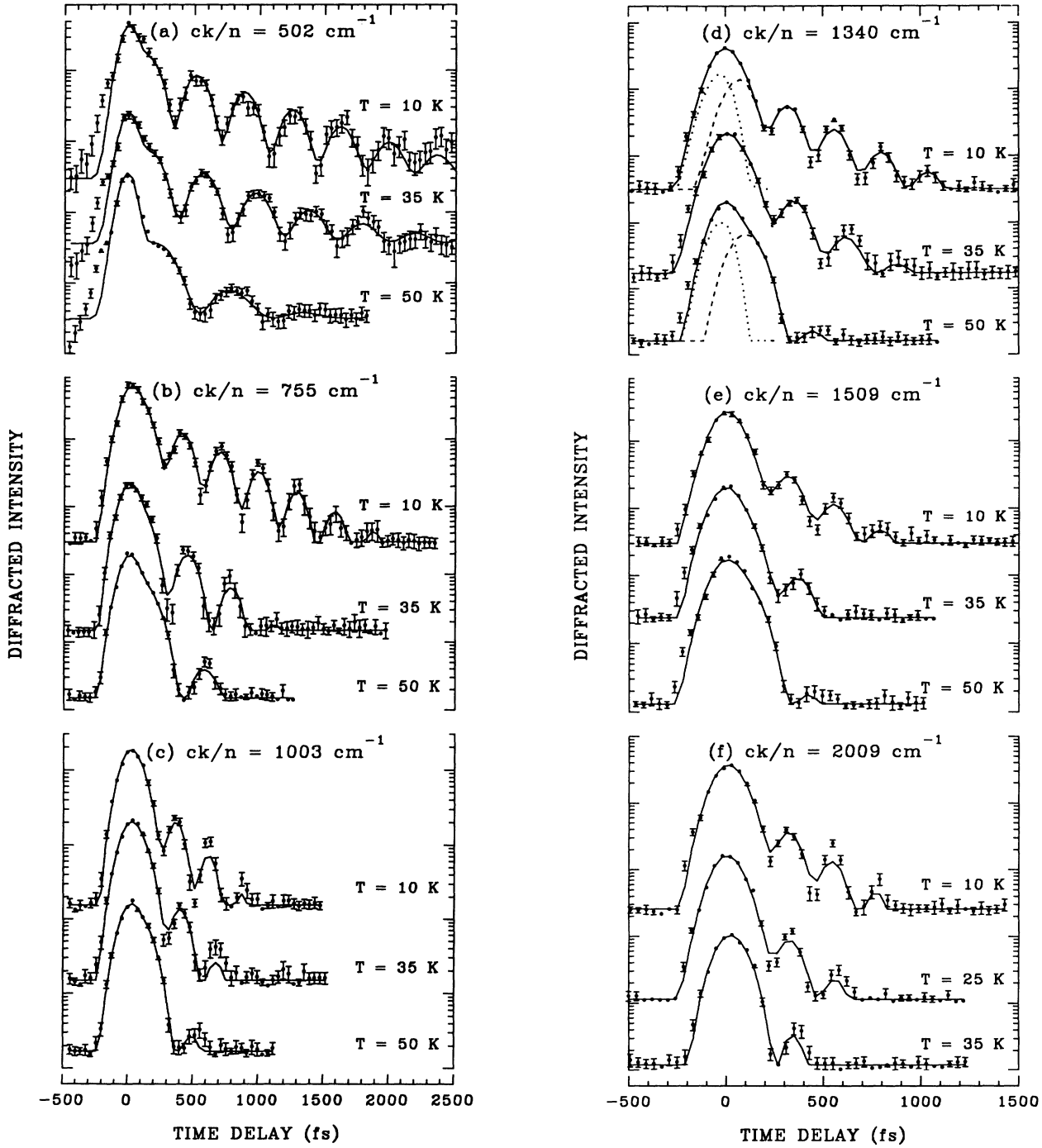

FIG. 1. Intensity of the ISS-diffracted signal as a function of the time delay between the pump and probe pulses for different temperatures and wave vectors. Symbols are the experimental data and the solid lines are theoretical fit with Eq. (2.1). On curves $T = 10$ K and $T = 50$ K of (d), the dotted and dashed lines are, respectively, the instantaneous and the polariton response contributions to the signal.

venience, as a function of the bare polariton frequency [ω_{k1}, Eq. (A6)]. Since $\tilde{\omega}_{k1}$ and ω_{k1} are related to k, by the experimental results and the polariton model, respectively, we may use indifferently k, $\tilde{\omega}_{k1}$, or ω_{k1} as the independent variable, keeping in mind that $\Sigma(\mathbf{k},\omega)$ values are deduced at $\omega = \tilde{\omega}_{k1}$.

As discussed in Sec. II, this calculation depends mainly on Ω_p. We choose $\Omega_p = 771$ cm^{-1} and take the values for ω_{TO} obtained from Raman scattering measurements. Consequently, at $T = 10$ K the real part of the phonon self-energy [Fig. 3(a)] does not vary significantly with ω_{k1} and is slightly below zero, since the Raman ω_{TO} value is smaller than the one obtained from the fit of the $T = 10$ K data [Fig. 2(a)].

While the real part of the self-energy at $T = 10$ K does not differ much from what we expect on the basis of the Raman scattering data, the imaginary part does, indeed, show a striking behavior. The dashed lines in Figs. 4(a) and 4(b) are the γ_{TO} values obtained from Raman scattering experiments.[21] There is a significant discrepancy between the constant γ_{TO} and $\Sigma^I(\mathbf{k},\omega)$ which is larger and is frequency dependent with a maximum around $\omega_{k1} \simeq 65$ cm^{-1} at $T = 10$ K (i.e., around $ck/n \simeq 1100$ cm^{-1}).

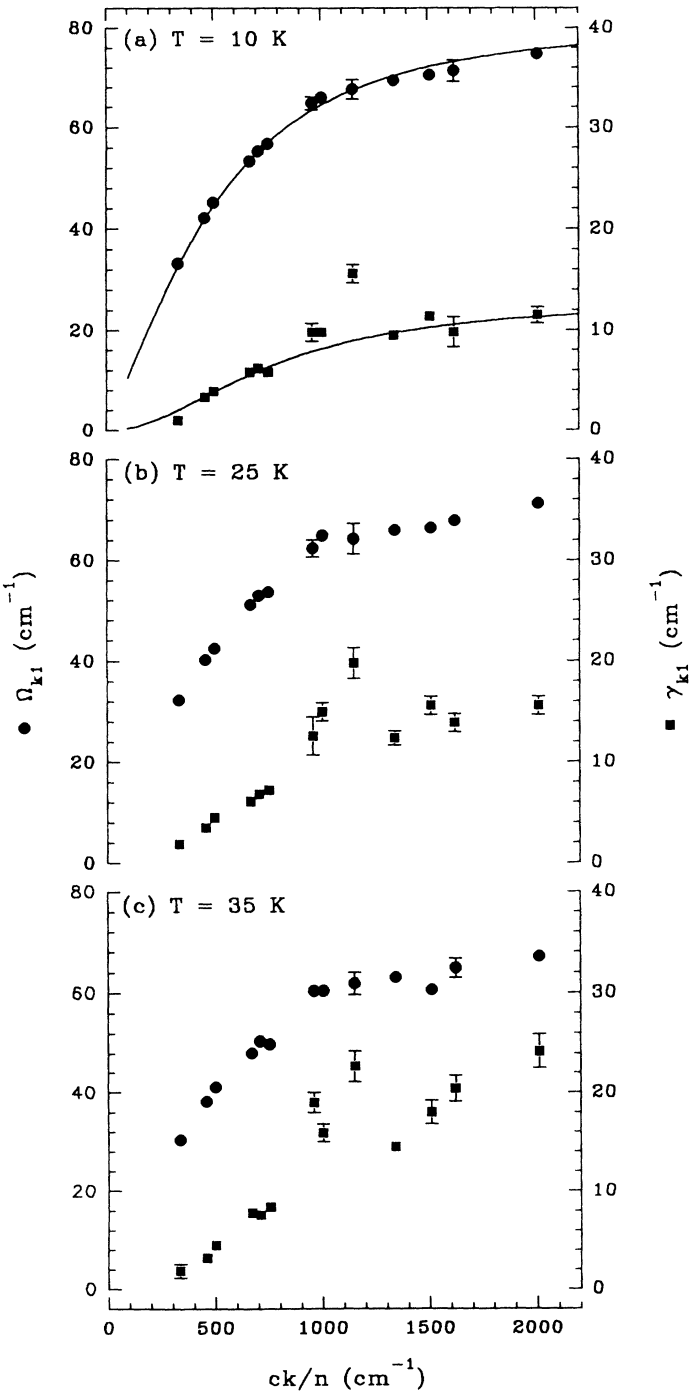

FIG. 2. Frequency Ω_{k1} (solid circle) and damping γ_{k1} (solid square) of the polariton as a function of wave vector for different temperatures. The solid line is a theoretical fit derived from Eq. (A17).

The polariton contribution to the ISS intensity as a function of k has also been determined. The results are presented in Figs. 5(a)–5(c). Since the absolute values of the scattering intensity may vary between two experiments, the values are normalized to the scattering intensity of the instantaneous part of the response (which is due to the virtual electronic excitation). As shown in Fig. 1(d), the polariton response and the instantaneous contributions are clearly distinguishable, making this normalization procedure reliable. The solid curves in Figs. 5(a)–5(c) are least-squares fits made using Eq. (B6) to compute the polariton-scattering amplitude with the experimental values of $\tilde{\omega}_{k1}$ and $\Sigma(\mathbf{k},\omega)$. The Raman and electro-optic tensors, obtained from those fits, are presented in Figs. 6(a) and 6(b), respectively.

V. DISCUSSION

A. Phonon self-energy $\Sigma(\mathbf{k},\omega)$

The first observation concerning the self-energy frequency dependence [see Figs. 3(a)–3(c) and Figs. 4(a)–

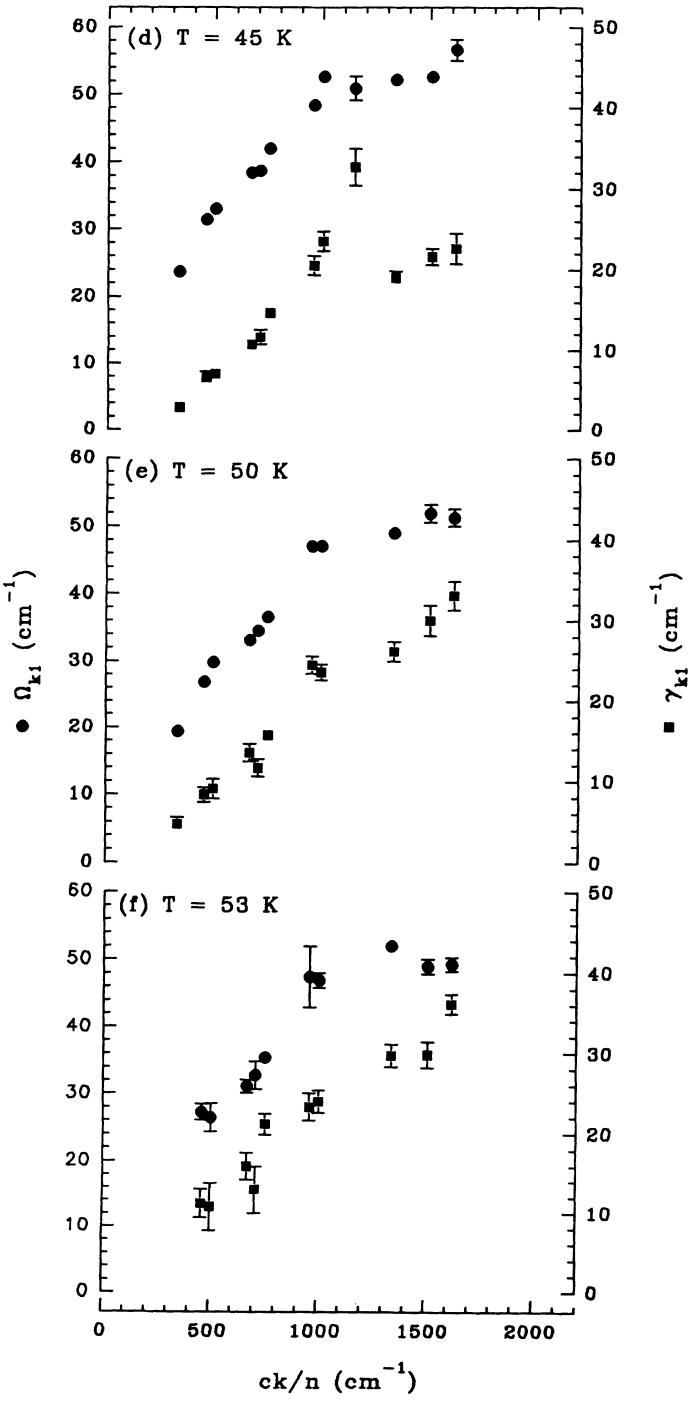

FIG. 2. (*Continued*).

4(c)] is the presence of structures at $ck/n \simeq 1100$ cm^{-1}, i.e., at $\omega_{k1} \simeq 65$ cm^{-1}, when $T = 10$ K. Such a maximum in the polariton damping rate has been observed in GaP (Refs. 22, 23) and results from the fact that the polariton frequency, at this particular wave vector, coincides with a combination of two or more elementary excitations. The self-energy, resulting from three particle interactions given by Eq. (A13), is resonantly enhanced. Detailed discussions of such a polariton anharmonic interaction with phonons have been presented recently by Vallée and Flytzanis.[24] From Figs. 4(a) and 4(b), it appears that, as a function of temperature, the maximum shifts at lower frequency, from $\omega_{k1} \simeq 65$ cm^{-1} at $T = 10$ K to $\omega_{k1} \simeq 54$ cm^{-1} at $T = 45$ K. This means that the phonons involved in the interaction should also soften as $T \rightarrow T_c$ similar to some acoustical branches as ob-

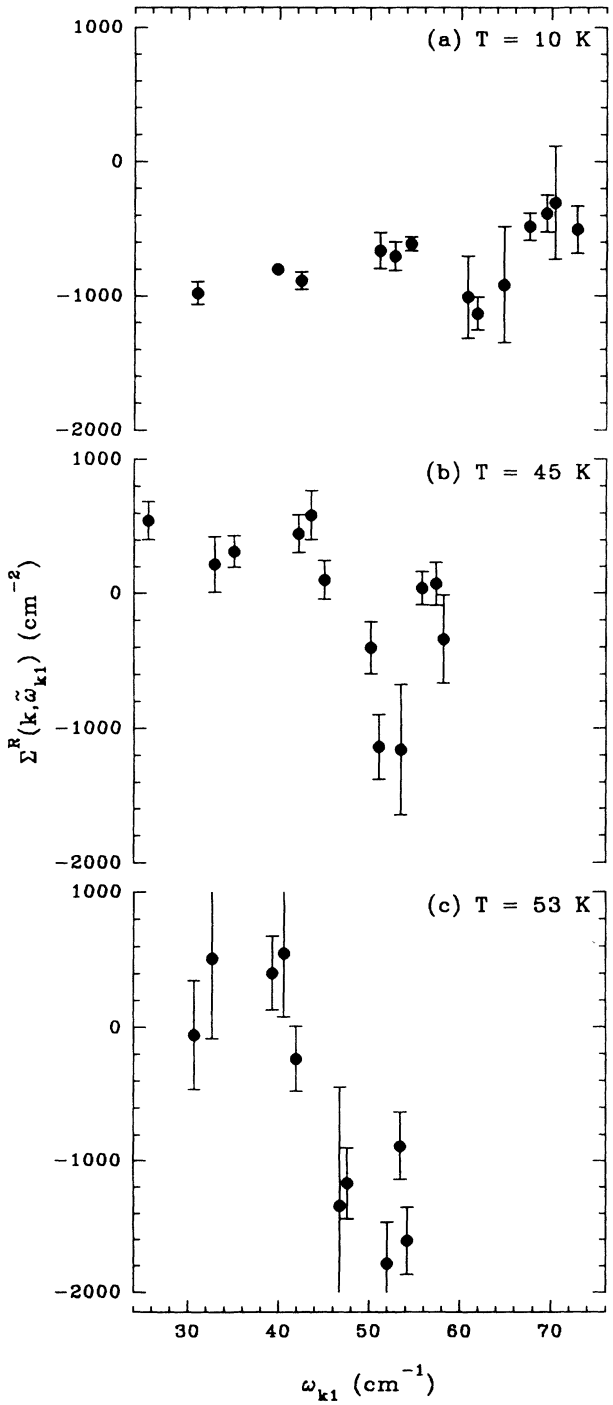

FIG. 3. Values of the real part of the phonon self-energy as a function of the polariton bare frequency (ω_{k1}) for different temperatures.

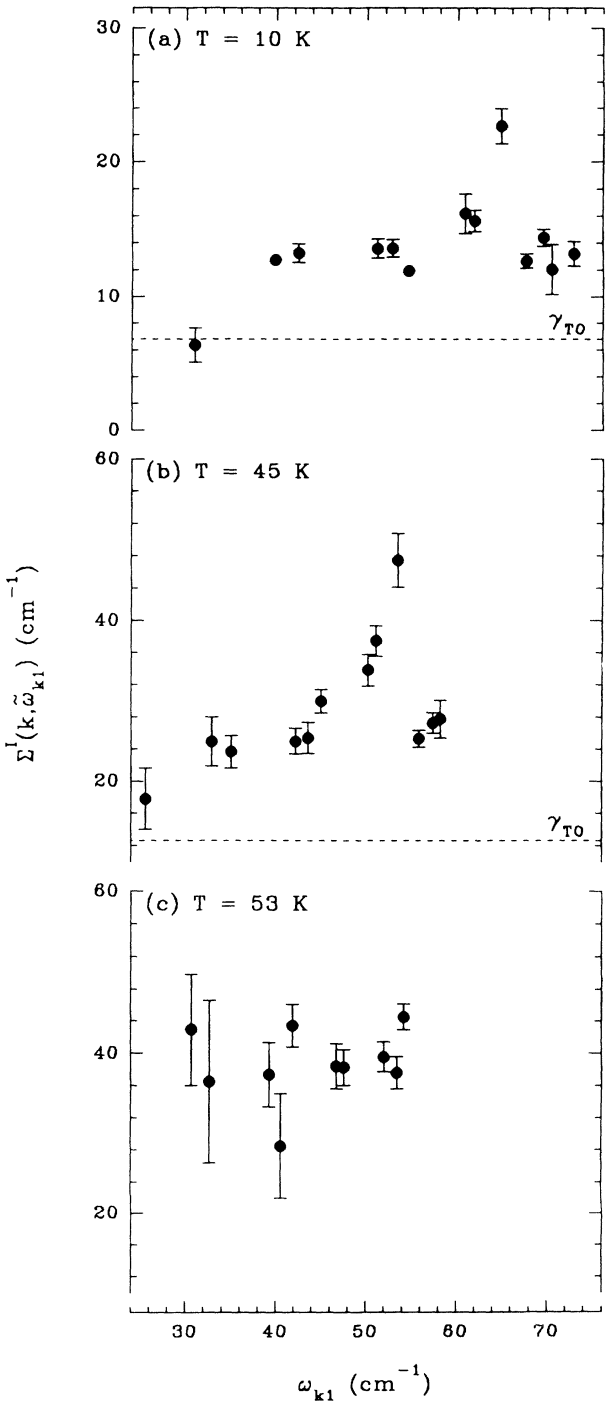

FIG. 4. Values of the imaginary part of the phonon self-energy as a function of the polariton bare frequency (ω_{k1}) for different temperatures. The dashed line represents the Raman phonon damping value.

served in KTN by Fontana *et al.*[25] and in $KTaO_3$ by Perry *et al.*[26] However, for a three-particle process, no optical-acoustical-phonon combination can be easily deduced from the dispersion curves.[26] We favor a process where two polaritons combine to generate two transverse-acoustical phonons at X or M point symmetry of the Brillouin zone. A strong resonance interaction occurs since the polariton at $ck/n \simeq 1100$ cm^{-1} and the former acoustical phonons have almost the same energy and also the same softening character.

Recent experimental investigations[4,27] attribute the A_1(TO) anomalous damping to its strong anharmonicity. Bakker *et al.*[4] showed that an anharmonic potential in $LiTaO_3$ gives rise to a resonance at a lower frequency than the main absorption. This new resonance leads to an additional peak in the dielectric response function imaginary part and a dip in its real part.

In order to compare those results to ours, we note that the following phenomenological expression has been used to describe the phonon self-energy resulting from a coupling to some low-lying states such as acoustical phonons:[28,29]

$$\Sigma(\omega) = \frac{b^2}{(\omega_A^2 - \omega^2) - 2i\omega\gamma_A} , \tag{5.1}$$

where ω_A and γ_A are the frequency and the damping that describe the particular decay process, with the coupling constant b. Thus a peak in the imaginary part of the self-energy and a dip in its real part are expected and here are measured for $\omega_A \simeq \omega_{k1}$ evaluated at $ck/n \simeq 1100$ cm^{-1}. If one calculates the dielectric response function associated with a phonon with such self-energy, given by[19]

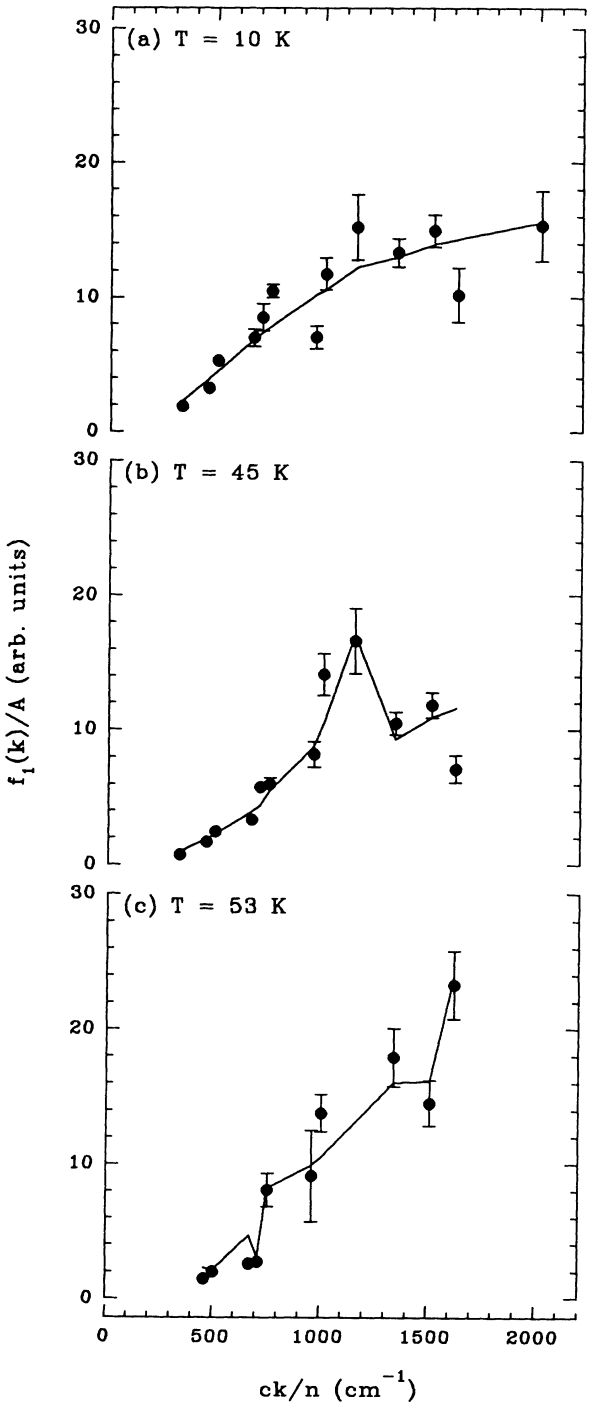

FIG. 5. Polariton diffraction intensity, as a function of wave vector for different temperatures, fitted with Eq. (B6) (solid line).

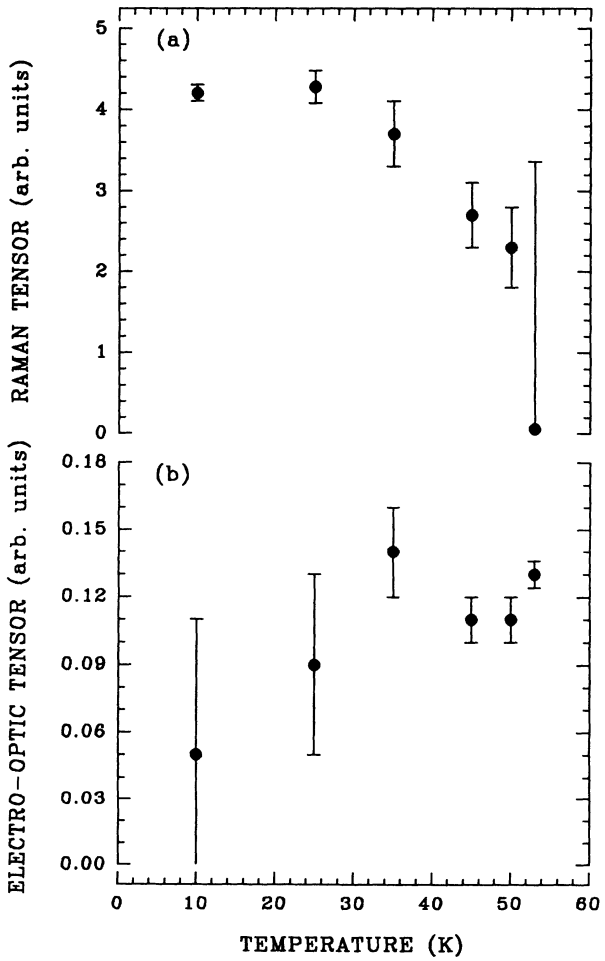

FIG. 6. Values of the Raman (a) and electro-optic (b) tensors for different temperatures.

$$\epsilon(\omega) \propto \chi(\omega) \propto \frac{1}{\omega_{\mathrm{TO}}^2 - \Sigma(\omega) - \omega^2} , \tag{5.2}$$

a similar frequency dependence to the one deduced by Bakker *et al.*[4] is obtained (except for the part associated with their relaxation mode).

It appears that the two formal approaches are, somehow, equivalent. In the one of Bakker *et al.*,[4] the anharmonicity is introduced, at the beginning, in the unit cell atomic potential. The consequences of such a potential on the response function are calculated and confirmed by their experimental results. In our case, we start with a harmonic model approximation (independent phonon) and the deviation of the experimental results from this model gives the anharmonicity, represented by a phonon-phonon interaction. The specific results in each study differ more than the used formal approach. In particular, frequency softening is absent in their case while here it shows up in the $A_1(\mathrm{TO})$ phonon frequency as well as in the frequency of the anharmonic interaction.

The other striking behavior of the self-energy imaginary part is that it appears to be larger than the Raman damping γ_{TO} by an approximately constant factor of 2 or more. Known factors affecting the measured damping rate in ISS such as the group velocity and the focal-point size[5,16,17,24] have been taken into account and discussed previously.[3,21] None of these could explain the observed discrepancy between the ISS and Raman scattering experiments. Damping rates larger by a factor of more than 2 in the polariton region (relative to what is predicted by the right-angle Raman scattering measurements) have also been observed in $LiTaO_3$ and $LiIO_3$.[5,24]

In the above discussion, concerning the maximum in the polariton damping rate, we have assumed that the self-energy is primarily a function of the polariton frequency and, consequently, of k through the dispersion relation. Excluding this maximum, the damping-rate behavior points towards a wave-vector dependence rather than a frequency dependence of the self-energy. More exactly, there seems to be a characteristic wave vector separating the two regions. The self-energy imaginary-part experimental values are approximately constant over the entire k or ω_{k1} range investigated here, that is, $ck/n \in [335\ \mathrm{cm}^{-1}, 2009\ \mathrm{cm}^{-1}]$ and $\omega_{k1} \in [32\ \mathrm{cm}^{-1}, 74\ \mathrm{cm}^{-1}]$ at $T = 10$ K. On the other hand, for a wave-vector transfer of $ck/n \simeq 27\,500\ \mathrm{cm}^{-1}$ the Raman scattering experiment gives $\omega_{\mathrm{TO}} \simeq 78\ \mathrm{cm}^{-1}$ at $T = 10$ K. Consequently, when calculating the self-energy, the only physical significative difference between the ISS and the Raman scattering experiments is the wave-vector transfer.

As a possible origin of this "exess" damping rate, we have considered the polariton-relaxation mode coupling (central-peak component). This interaction leads to the following form for the self-energy:[10,13–15]

$$\Sigma_{p-r}(\omega) = \frac{-\omega\delta^2}{\omega + i\gamma_r} , \tag{5.3}$$

where γ_r is the inverse relaxation time of the Debye-relaxation mode and δ is the coupling constant. For the usual value of γ_r,[10,13–15] one gets $\Sigma^R_{p-r} \sim -\delta^2$ and $\Sigma^I_{p-r} \sim \gamma_r\delta^2/(2\omega^2)$ which does not correspond to our measurements. For $LiTaO_3$, the central peak component is rather described by[4,30]

$$\Sigma_{p-r}(\omega) = \frac{i\gamma_r\delta^2}{\omega + i\gamma_r} , \tag{5.4}$$

which gives $\Sigma^R_{p-r} \sim \gamma_r^2\delta^2/\omega^2$ and $\Sigma^I_{p-r} \sim \gamma_r\delta^2/(2\omega)$. While it may explain the observed variation in $\Sigma^R(\mathbf{k},\omega)$ at T near T_c [see Fig. 3(c)], it does not reproduce the variation of $\Sigma^I(\mathbf{k},\omega)$. Also, we have calculated the damping resulting from a correction to the phonon-photon interaction through an effective polariton-polariton interaction, as done by Mavroyannis *et al.*[31,32] Such polariton self-energy does not fit the k dependence observed here.

The imperfect "monodomain" structure of the sample could be at the origin of the observed discrepancy. As discussed previously in Ref. 21, we have excluded the possibility of having both soft-phonon modes A_1 and E_g contributing to the ISS signal and to an apparent damping rate larger than expected. The difference introduced by the microdomain structure should be rather related to the typical wavelength of the probed polariton mode in the ISS and the phonon mode in the Raman scattering experiments. The polariton wavelength generated and probed in the present ISS experiment is between 2.2 and 13.3 μm, while for right-angle Raman scattering, the probed phonon wavelength is typically 0.16 μm. If the microdomain dimensions are close to the polariton wavelength, clearly the ISS technique will be more sensitive to this structure.

While some experiments have undoubtedly demonstrated the presence of impurity-induced ferroelectric microdomains in highly polarizable perovskite crystals such as $KTaO_3$,[33–35] the effect of Nb impurities in relation to the phase transition is less clear. However, it is now accepted that the Nb ions are at an off-center position.[11,12] Thereby, polarized regions of increasing size as $T \to T_c$ are formed around the Nb-dipole impurities. Evidence for a coexistence of the ferroelectric and dipolar glass states has been put forward by Toulouse *et al.*[36,37] Depolarization experiments clearly demonstrate the existence in KTN of ferroelectric domains with dimensions exceeding 0.5 μm.[38] The presence of such clusters has also been considered as a possible explanation for the anomalies in the behavior of the soft TO and TA phonon branches as a function of wave vector and temperature.[25] It is quite plausible that the discrepancy between the Raman scattering and the ISS experiments is due to the relatively larger spatial extension of the polariton wave packet that renders it more sensitive to the ferroelectric microdomains. Thus, the Raman scattering results would be related more to the intracluster dynamics while in the ISS measurement long-range intercluster dynamics would be probed.

B. Wave-vector dependence of the ISS intensity

The maximum appearing in the self-energy at $ck/n \simeq 1100\ \mathrm{cm}^{-1}$ is also present in the intensity measurement; see Figs. 5(a) and 5(b). A maximum also appears in the theoretical evaluation of the polariton-response-

function amplitude $f_1(k)$, as shown in Fig. 7(a), when the scattering intensity is dominated by the electro-optic tensor contribution. This maximum is at smaller k ($ck/n \simeq 500$ cm^{-1}) and a much higher Ω_p value is needed to displace it up to a value of $ck/n \simeq 1100$ cm^{-1}. Consequently, the observed maximum is not really related to this phenomenon. Thus, since it is not reproduced by the simple polariton model with a constant $\Sigma^I(\mathbf{k},\omega)$, this maximum confirms the presence of an additional interaction, leading to the features observed in the self-energy and the ISS-intensity data. If we use the experimental values for the pole $\tilde{\omega}_{k1}$ and the deduced self-energy, an accurate reproduction of the ISS scattering-intensity k dependence is obtained [see the solid curves in Figs. 5(a)–5(c)].

The Raman and electro-optic tensors, obtained from the least-squares fits to the ISS-intensity data, are presented in Figs. 6(a) and 6(b), respectively. At $T = 10$ K, only a Raman-tensor value is needed to the fit. When $T \rightarrow T_c$ the Raman contribution decreases, while the electro-optic tensor contribution increases and becomes dominant at $T = 53$ K.

The Raman tensor decreases, as $T \rightarrow T_c$, following the soft-phonon frequency behavior. This is consistent with the lattice dynamics described by the core-shell model of Migoni *et al.*[39] where the oxygen polarizability decreases in the O-Ta(Nb) direction as $T \rightarrow T_c$.[40,41] Our results [Figs. 6(a) and 6(b)] also indicate clearly that, as $T \rightarrow T_c$, the soft mode is coupled to the electronic polarizability mainly through the electro-optic tensor, showing thus the importance of the electromagnetic interaction in the soft-phonon dynamics close to T_c. This favors the model of Vugmeister *et al.*,[11,42,43] where the dipolar interaction between clusters induced by the off-center Nb subsitution ion drives the ferroelectric phase transition.

VI. CONCLUSIONS

The results of an ISS investigation of the A_1 soft-polariton mode as a function of temperature and wave vector are presented. Based on a simple polariton model, the phonon self-energy wave-vector dependence, the Raman tensor, and the electro-optic tensor are deduced from the measured polariton frequency, damping rate, and diffraction intensity.

Results for the phonon self-energy differ from what one might expect based on Raman scattering experiments, indicating the existence of an additional interaction in the polariton regime. Two anomalous features were observed in the phonon self-energy imaginary part. First, the presence of a maximum which we tentatively attribute to a four-particle interaction-relaxation process. Second, the phonon damping at small wave vector (in the polariton region) is larger than the Raman value by approximately a constant factor of 2 or more. The most probable explanation is the existence of ferroelectric domains with a characteristic length that is comparable to the polariton wavelength investigated in the present ISS experiment. This should result in an essential difference in the dynamical properties probed by a right-angle Raman scattering experiment. In the latter, intracluster dymanics are probed while, in the former, the intercluster dynamics dominate in the response of the system.

Results for the Raman and electro-optic tensors as a function of temperature indicate the predominance of the electromagnetic interaction in the long-range intercluster dynamics close to T_c.

These results show the ability of the ISS experimental technique to probe the nature of the long-range interaction in such system. It should be interesting to see how such measurement evolves with the Nb concentration in KTN since it is believed that a crossover from an order-disorder-type phase transition to a displacive phase transition takes place with increasing concentration.[42]

ACKNOWLEDGMENTS

The research performed at l'Université de Sherbrooke was supported by the Medical Research Council of Canada, the Center of Excellence in Molecular and Interfacial Dynamic, and le fonds pour la Formation des Chercheurs et l'Aide à la Recherche. Research performed at the Oak Ridge National Laboratory, Solid State Division, is supported by the Division of Materials Sciences, U.S. Department of Energy, under Contract No. DE–AC0584OR21400 with Mariette Systems, Inc.

APPENDIX A

Here we present, in some detail, the diagonalization of the phonon-photon Hamiltonian by the introduction of the creation and annihilation polariton operators. This is required for two reasons: First, we need an explicit expression to relate the experimentally observed frequency and damping rate of the polariton to the phonon characteristics. Second, we believe that there are some mistakes in the previous published works on such topics.

Following the notation of Benson and Mills,[44] the phonon and photon Hamiltonian, in the case where only one phonon branch j_0 interacts with the transverse photon of polarization λ, is

$$H = \frac{1}{2}\sum_{\mathbf{k}}(P^{\dagger}_{\mathbf{k}j_0}P_{\mathbf{k}j_0} + \omega^2_{\mathrm{TO}}Q^{\dagger}_{\mathbf{k}j_0}Q_{\mathbf{k}j_0}) + \frac{1}{2}\sum_{\mathbf{k}}\left(\Pi^{\dagger}_{\mathbf{k}\lambda}\Pi_{\mathbf{k}\lambda} + \frac{c^2k^2}{n^2}A^{\dagger}_{\mathbf{k}\lambda}A_{\mathbf{k}\lambda}\right) - \Omega_p\sum_{\mathbf{k}}P^{\dagger}_{\mathbf{k}j_0}A_{\mathbf{k}\lambda} + \frac{\Omega_p^2}{2}\sum_{\mathbf{k}}A^{\dagger}_{\mathbf{k}\lambda}A_{\mathbf{k}\lambda}\ , \tag{A1}$$

where Ω_p is the ionic plasma frequency related within the Lyddane-Sachs-Teller relation to the transverse (ω_{TO}) and the longitudinal (ω_{LO}) phonon frequency by the relation $\Omega_p^2 = \omega^2_{\mathrm{LO}} - \omega^2_{\mathrm{TO}}$. The following definitions have been used for the operators:

$$Q_{\mathbf{k}j_0} = \left(\frac{\hbar}{2\omega_{\mathrm{TO}}}\right)^{1/2}(b_{\mathbf{k}j_0} + b^{\dagger}_{-\mathbf{k}j_0})\ , \tag{A2a}$$

$$P_{\mathbf{k}j_0} = i\left(\frac{\hbar\omega_{\mathrm{TO}}}{2}\right)^{1/2}(b_{\mathbf{k}j_0} - b^{\dagger}_{-\mathbf{k}j_0})\ , \tag{A2b}$$

$$A_{\mathbf{k}\lambda} = \left(\frac{\hbar}{2ck/n}\right)^{1/2} (a_{\mathbf{k}\lambda} + a^{\dagger}_{-\mathbf{k}\lambda}) \ , \tag{A2c}$$

$$\Pi_{\mathbf{k}\lambda} = i\left(\frac{\hbar ck/n}{2}\right)^{1/2} (a_{\mathbf{k}\lambda} - a^{\dagger}_{-\mathbf{k}\lambda}) \ , \tag{A2d}$$

where $a^{\dagger}_{\mathbf{k}\lambda}$, $a_{\mathbf{k}\lambda}$ and $b^{\dagger}_{\mathbf{k}j_0}$, $b_{\mathbf{k}j_0}$ are the creation and annihilation operators for the photon and phonon, respectively.

This Hamiltonian [Eq. (A1)] can be diagonalized with a canonical transformation to exhibit the independent polariton modes,[45,46] leading to a Hamiltonian of the form

$$H = \sum_{\mathbf{k}\rho} \hbar\omega_{k\rho}\alpha^{\dagger}_{\mathbf{k}\rho}\alpha_{\mathbf{k}\rho} \ . \tag{A3}$$

With the appropriate choice of phase, one obtains the following relation between the phonon and photon operators and the polariton operators:

$$Q_{\mathbf{k}j_0} = \sum_{\rho} \left[S^{Q}_{\rho}(k)\right]^{1/2} \left(\frac{\omega_{k\rho}}{\omega_{\mathrm{TO}}}\right)^{1/2} \widetilde{A}_{\mathbf{k}\rho} \ , \tag{A4a}$$

$$P_{\mathbf{k}j_0} = \sum_{\rho} [S^{P}_{\rho}(k)]^{1/2} \left(\frac{\omega_{\mathrm{TO}}}{\omega_{k\rho}}\right)^{1/2} \widetilde{P}_{\mathbf{k}\rho} \ , \tag{A4b}$$

$$A_{\mathbf{k}\lambda} = \sum_{\rho} (-1)^{\rho+1} \left[S^{A}_{\rho}(k)\right]^{1/2} \left(\frac{1}{\omega_{k\rho}ck/n}\right)^{1/2} \widetilde{P}_{\mathbf{k}\rho} \ , \tag{A4c}$$

$$\Pi_{\mathbf{k}\lambda} = \sum_{\rho} (-1)^{\rho} \left[S^{\Pi}_{\rho}(k)\right]^{1/2} (\omega_{k\rho}ck/n)^{1/2} \widetilde{A}_{\mathbf{k}\rho} \ , \tag{A4d}$$

where the operators $\widetilde{A}_{\mathbf{k}\rho}$ and $\widetilde{P}_{\mathbf{k}\rho}$ are defined in terms of the creation and annihilation polariton operators ($\alpha^{\dagger}_{\mathbf{k}\rho}$, $\alpha_{\mathbf{k}\rho}$) as

$$\widetilde{A}_{\mathbf{k}\rho} = \left(\frac{\hbar}{2\omega_{k\rho}}\right)^{1/2} (\alpha_{\mathbf{k}\rho} + \alpha^{\dagger}_{-\mathbf{k}\rho}) \ , \tag{A5a}$$

$$\widetilde{P}_{\mathbf{k}\rho} = i\left(\frac{\hbar\omega_{k\rho}}{2}\right)^{1/2} (\alpha_{\mathbf{k}\rho} - \alpha^{\dagger}_{-\mathbf{k}\rho}) \ . \tag{A5b}$$

The bare polariton frequency ($\omega_{k\rho}$) is given by

$$\omega_{k\rho=1,2} = \frac{1}{\sqrt{2}} \left\{ \frac{c^2k^2}{n^2} + \Omega_p^2 + \omega_{\mathrm{TO}}^2 \pm \left[\left(\frac{c^2k^2}{n^2} + \Omega_p^2 + \omega_{\mathrm{TO}}^2 \right)^2 - 4\frac{c^2k^2}{n^2}\omega_{\mathrm{TO}}^2 \right]^{1/2} \right\}^{1/2} \ , \tag{A6}$$

and the factors $S^{(X)}_{\rho}(k)$ represent the strength function,

$$S^{Q}_{\rho}(k) = \frac{\Omega_p^2\omega_{\mathrm{TO}}\omega_{k\rho}}{[(\omega_{\mathrm{TO}}^2 - \omega_{k\rho}^2)^2 + \Omega_p^2\omega_{\mathrm{TO}}^2]} \ , \tag{A7a}$$

$$S^{P}_{\rho}(k) = \frac{\Omega_p^2\omega_{\mathrm{TO}}^3}{\omega_{k\rho}[(\omega_{\mathrm{TO}}^2 - \omega_{k\rho}^2)^2 + \Omega_p^2\omega_{\mathrm{TO}}^2]} \ , \tag{A7b}$$

$$S^{A}_{\rho}(k) = \frac{ck/n(\omega_{\mathrm{TO}}^2 - \omega_{k\rho}^2)^2}{\omega_{k\rho}[(\omega_{\mathrm{TO}}^2 - \omega_{k\rho}^2)^2 + \Omega_p^2\omega_{\mathrm{TO}}^2]} \ , \tag{A7c}$$

$$S^{\Pi}_{\rho}(k) = \frac{\omega_{k\rho}(\omega_{\mathrm{TO}}^2 - \omega_{k\rho}^2)^2}{ck/n[(\omega_{\mathrm{TO}}^2 - \omega_{k\rho}^2)^2 + \Omega_p^2\omega_{\mathrm{TO}}^2]} \ ; \tag{A7d}$$

these are the same factors deduced by other authors.[31,32,47,48]

In order to introduce the polariton lifetime, we proceed following Vallée and Flytzanis.[24] Starting with a Hamiltonian that describes a phonon-phonon interaction through the third-order mechanical anharmonicity,

$$H_{\mathrm{int}} = \sum_{\substack{\mathbf{kq} \\ j_1j_2j_3}} V_3(\mathbf{k}, j_1; \mathbf{q}, j_2; -\mathbf{q}-\mathbf{k}, j_3) \times Q_{\mathbf{k}j_1} Q_{\mathbf{q}j_2} Q_{-\mathbf{q}-\mathbf{k}j_3} \ , \tag{A8}$$

the expression becomes [with Eq. (A4a)]:

$$H_{\mathrm{int}} = \sum_{\substack{\mathbf{kq} \\ \rho j_2 j_3}} V_3(\mathbf{k}, j_0; \mathbf{q}, j_2; -\mathbf{q}-\mathbf{k}, j_3) \left[S^{Q}_{\rho}(k)\right]^{1/2} \times \left(\frac{\omega_{k\rho}}{\omega_{\mathrm{TO}}}\right)^{1/2} \widetilde{A}_{\mathbf{k}\rho} Q_{\mathbf{q}j_2} Q_{-\mathbf{q}-\mathbf{k}j_3} \ , \tag{A9}$$

in terms of the polariton operators with one phonon originating from the j_0 branch. Using the standard procedure,[18] one obtains a Dyson equation for the polariton propagators,

$$\begin{pmatrix} G^{11} & G^{12} \\ G^{21} & G^{22} \end{pmatrix} = \begin{pmatrix} G_0^{11} & 0 \\ 0 & G_0^{22} \end{pmatrix} + \begin{pmatrix} G^{11} & G^{12} \\ G^{21} & G^{22} \end{pmatrix} \begin{pmatrix} G_0^{11} S_1^{Q} \frac{\omega_{k_1}}{\omega_{\mathrm{TO}}} \Sigma & G_0^{22} \frac{(S_1^{Q}\omega_{k_1} S_2^{Q}\omega_{k_2})^{1/2}}{\omega_{\mathrm{TO}}} \Sigma \\ G_0^{11} \frac{(S_1^{Q}\omega_{k_1} S_2^{Q}\omega_{k_2})^{1/2}}{\omega_{\mathrm{TO}}} \Sigma & G_0^{22} S_2^{Q} \frac{\omega_{k_2}}{\omega_{\mathrm{TO}}} \Sigma \end{pmatrix} \ , \tag{A10}$$

where $G^{ij} \equiv G^{\widetilde{A}_{\rho=i}\widetilde{A}_{\rho=j}}(\mathbf{k}, \omega)$ are the polariton propagators defined in the following way:

$$G^{\widetilde{A}_{\rho}\widetilde{A}_{\rho'}}(\mathbf{k}, t-t') = \frac{i}{\hbar} \langle [\widetilde{A}_{\mathbf{k}\rho}(t), \widetilde{A}^{\dagger}_{\mathbf{k}\rho'}(t')] \rangle \Theta(t-t') \ . \tag{A11}$$

Thus the bare polariton propagators (G_0^{ii}) become

$$G_0^{ii}(\mathbf{k}, \omega) = \frac{1}{\omega_{k\rho=i}^2 - \omega^2} \ . \tag{A12}$$

$\Sigma \equiv \Sigma(\mathbf{k}, \omega)$ in Eq. (A10) are the self-energy bubbles that involve phonon propagators from branches other than the j_0 branch. To the lowest-order perturbation theory leading to a lifetime,[19,49] we get

$$\Sigma(\mathbf{k},i\omega)=18\sum_{\mathbf{q}j_2j_3}|V_3(-\mathbf{k},j_0;\mathbf{q},j_2;\mathbf{k}-\mathbf{q},j_3)|^2\frac{1}{\beta\hbar}\sum_{i\omega_n}G_0^{QQ}(\mathbf{q},j_2;i\omega_n)G_0^{QQ}(\mathbf{k}-\mathbf{q},j_3;i\omega-i\omega_n)\ . \tag{A13}$$

Solving Eq. (A10) and neglecting Σ^2 term in the denominator, we obtain

$$G^{11}=\frac{\omega_{k2}^2-\omega^2-S_2^Q(k)\frac{\omega_{k2}}{\omega_{\rm TO}}\Sigma}{D}\ , \tag{A14a}$$

$$G^{12}=G^{21}=\frac{\left[S_1^Q(k)\frac{\omega_{k1}}{\omega_{\rm TO}}S_2^Q(k)\frac{\omega_{k2}}{\omega_{\rm TO}}\right]^{1/2}\Sigma}{D}\ , \tag{A14b}$$

$$G^{22}=\frac{\omega_{k1}^2-\omega^2-S_1^Q(k)\frac{\omega_{k1}}{\omega_{\rm TO}}\Sigma}{D}\ , \tag{A14c}$$

where

$$D=\left(\omega_{k1}^2-S_1^Q(k)\frac{\omega_{k1}}{\omega_{\rm TO}}\Sigma-\omega^2\right)\times\left(\omega_{k2}^2-S_2^Q(k)\frac{\omega_{k2}}{\omega_{\rm TO}}\Sigma-\omega^2\right)\ . \tag{A15}$$

Consequently, the polariton self-energy $[\widetilde{\Sigma}(\mathbf{k}\rho,\omega)]$ is related to the phonon self-energy $[\Sigma(\mathbf{k},\omega)]$ by

$$\widetilde{\Sigma}(\mathbf{k}\rho,\omega)=S_\rho^Q(k)\frac{\omega_{k\rho}}{\omega_{\rm TO}}\Sigma(\mathbf{k},\omega)\ . \tag{A16}$$

This result differs from previous work[24,47] by the extra factor $\omega_{k\rho}/\omega_{\rm TO}$. It is not solely related to the propagator normalization used here [Eqs. (A2a)–(A2d) and (A5a)–(A5b)], since without the normalization, these frequencies would appear in the numerator of the propagators.

Separating the phonon self-energy into real and imaginary parts and using the fact that the imaginary part is odd in ω, we find

$$\Sigma(\mathbf{k},\omega)=\Sigma^R(\mathbf{k},\omega)+2i\omega\Sigma^I(\mathbf{k},\omega)\ ;$$

the propagator poles are, thus, located at

$$\widetilde{\omega}_{k\rho}=\pm\left[\omega_{k\rho}^2-S_\rho^Q(k)\frac{\omega_{k\rho}}{\omega_{\rm TO}}\Sigma^R(\mathbf{k},\omega=\widetilde{\omega}_{k\rho})-\left(S_\rho^Q(k)\frac{\omega_{k\rho}}{\omega_{\rm TO}}\Sigma^I(\mathbf{k},\omega=\widetilde{\omega}_{k\rho})\right)^2\right]^{1/2}-iS_\rho^Q(k)\frac{\omega_{k\rho}}{\omega_{\rm TO}}\Sigma^I(\mathbf{k},\omega=\widetilde{\omega}_{k\rho})\ . \tag{A17}$$

Using Eqs. (A4a)–(A4d) and (A14a)–(A14c), the phonon and the photon propagators associated to the polariton branch are obtained as follows:

$$G^{QQ}(\mathbf{k},\omega)=\left[S_1^Q(k)\frac{\omega_{k1}}{\omega_{\rm TO}}\left(\omega_{k2}^2-\omega^2\right)+S_2^Q(k)\frac{\omega_{k2}}{\omega_{\rm TO}}\left(\omega_{k1}^2-\omega^2\right)\right]D^{-1}\ , \tag{A18a}$$

$$G^{Q\Pi}(\mathbf{k},\omega)=G^{\Pi Q}(\mathbf{k},\omega)=\left[-\left(S_1^Q(k)\frac{\omega_{k1}}{\omega_{\rm TO}}S_1^\Pi(k)\omega_{k1}ck/n\right)^{1/2}\left(\omega_{k2}^2-\omega^2\right)+\left(S_2^Q(k)\frac{\omega_{k2}}{\omega_{\rm TO}}S_2^\Pi(k)\omega_{k2}ck/n\right)^{1/2}\left(\omega_{k1}^2-\omega^2\right)\right]D^{-1}\ , \tag{A18b}$$

$$G^{\Pi\Pi}(\mathbf{k},\omega)=\left\{S_1^\Pi(k)\omega_{k1}ck/n\left(\omega_{k2}^2-\omega^2\right)+S_2^\Pi(k)\omega_{k2}ck/n\left(\omega_{k1}^2-\omega^2\right)-\left[\left(S_1^Q(k)\frac{\omega_{k1}}{\omega_{\rm TO}}S_2^\Pi(k)\omega_{k2}ck/n\right)^{1/2}+\left(S_2^Q(k)\frac{\omega_{k2}}{\omega_{\rm TO}}S_1^\Pi(k)\omega_{k1}ck/n\right)^{1/2}\right]^2\Sigma\right\}D^{-1}\ . \tag{A18c}$$

Equivalent results could be obtained using the method presented by Benson and Mills.[44] The advantage of the method given here is that we obtain an analytical expression relating the polariton self-energy to the phonon self-energy [Eq. (A16)], while in the former method, an explicit expression for the phonon self-energy has to be postulated in order to evaluate numerically the polariton propagator poles.

APPENDIX B

Here we present a generalization of the dielectric-constant impulse-response function calculation, related to the ISS experiment, with the formalism given in Appendix: A. According to the Yan-Nelson[16] calculation, it is possible to relate the diffraction efficiency to the dielectric-constant impulse-response function $G^{\epsilon\epsilon}(t)$ as

$$I(t)\propto|G^{\epsilon\epsilon}(t)|^2\ . \tag{B1}$$

$G^{\epsilon\epsilon}(t)$ is obtained through linear-response theory using the following generic interaction Hamiltonian:

$$H_1=-\frac{1}{2}\int d\mathbf{r}\sum_{ij}\epsilon_{ij}(\mathbf{r})E_i(\mathbf{r})E_j(\mathbf{r})\ , \tag{B2}$$

which gives

$$G^{\epsilon\epsilon}_{ijkl}(\mathbf{k}, t-t') = \frac{i}{\hbar}\langle[\epsilon_{ij}(\mathbf{k},t), \epsilon_{kl}(-\mathbf{k},t')]\rangle\Theta(t-t') \ . \tag{B3}$$

The dielectric constant is coupled in two ways to the polariton mode. The first is the atomic displacement $[\mathbf{u}(\mathbf{r})]$ contribution (Raman effect) and the second is associated with the dependence of the dielectric constant on the electric field $[\mathbf{E}^{\Pi}(\mathbf{r})]$ of the excited polariton (electro-optic effect). The expression given by Benson and Mills[44] for the coupling of the radiation field to the polariton mode is

$$H_1 = -\frac{1}{2}\int d\mathbf{r} \sum_{ij;\gamma} \left[a_{ij;\gamma}u_\gamma(\mathbf{r}) + b_{ij;\gamma}E^{\Pi}_\gamma(\mathbf{r})\right] E_i(\mathbf{r})E_j(\mathbf{r}) \ . \tag{B4}$$

Then, using their definition of $\mathbf{u}(\mathbf{r})$ and $\mathbf{E}^{\Pi}(\mathbf{r})$, and considering all polarizations along the c axis with only one polariton mode of polarization $\gamma = c$ as in Appendix A, we obtain

$$G^{\epsilon\epsilon}_{cccc}(\mathbf{k},t) = a^2G^{QQ}(\mathbf{k},t) + abG^{Q\Pi}(\mathbf{k},t) + baG^{\Pi Q}(\mathbf{k},t) + b^2G^{\Pi\Pi}(\mathbf{k},t) \ , \tag{B5}$$

where

$$a = \left(\frac{V_c}{m}\right)^{1/2} a_{cc;c} \ , \quad b = \left(\frac{4\pi}{\epsilon_\infty}\right)^{1/2} b_{cc;c} \ ;$$

V_c is the unit cell volume and m the oscillator effective mass. Then, using Eqs. (A18a)–(A18c), we get

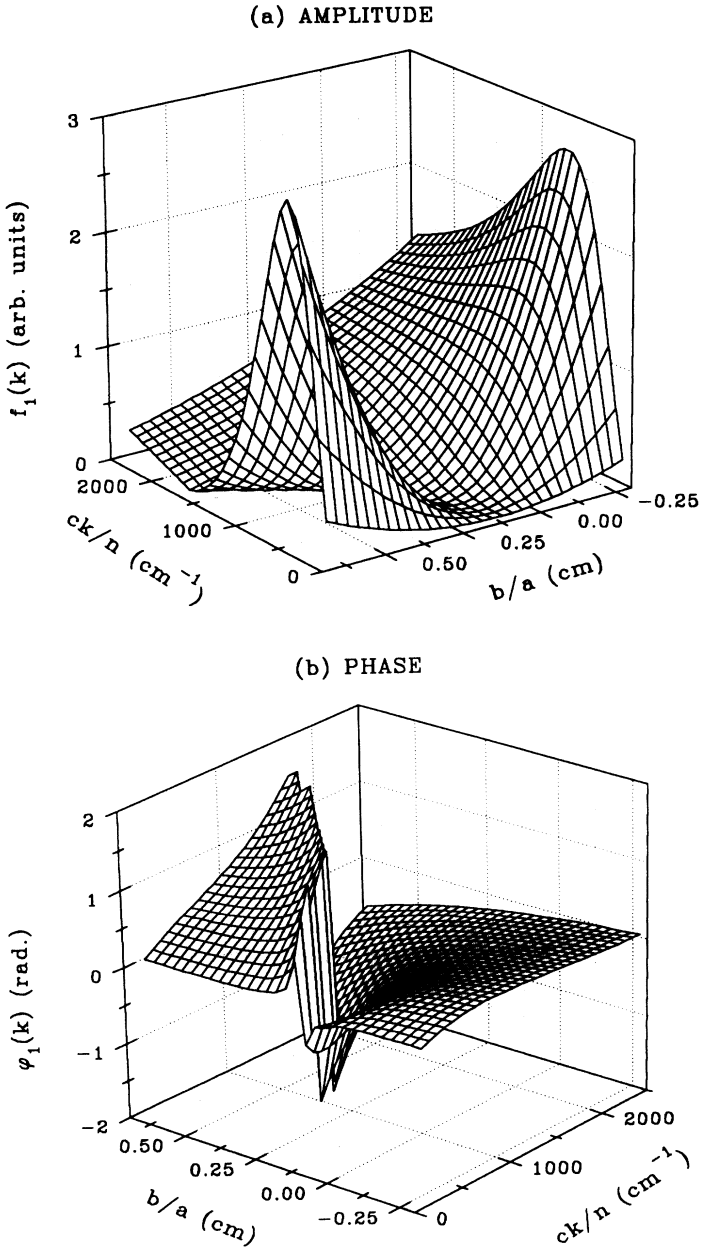

FIG. 7. Calculated polariton response function, amplitude (a), and phase (b), as a function of wave vector and relative strength of the Raman a and the electro-optic b tensors.

$$G^{\epsilon\epsilon}_{cccc}(\mathbf{k},\omega) = \left\{ \left[a\left(S_1^Q(k)\frac{\omega_{k1}}{\omega_{\rm TO}} \right)^{1/2} - b\left(S_1^\Pi(k)\omega_{k1}ck/n \right)^{1/2} \right]^2 (\omega_{k2}^2 - \omega^2) \right.$$
$$+ \left[a\left(S_2^Q(k)\frac{\omega_{k2}}{\omega_{\rm TO}} \right)^{1/2} + b\left(S_2^\Pi(k)\omega_{k2}ck/n \right)^{1/2} \right]^2 (\omega_{k1}^2 - \omega^2)$$
$$\left. -b^2 \left[\left(S_1^Q(k)\frac{\omega_{k1}}{\omega_{\rm TO}} S_2^\Pi \omega_{k2}ck/n \right)^{1/2} + \left(S_2^Q(k)\frac{\omega_{k2}}{\omega_{\rm TO}} S_1^\Pi \omega_{k1}ck/n \right)^{1/2} \right]^2 \Sigma \right\} D^{-1} . \quad \text{(B6)}$$

Given that the poles of $G^{\epsilon\epsilon}_{cccc}(\mathbf{k},\omega)$ are located at

$$\tilde{\omega}_{k\rho} = \pm\Omega_{k\rho} - i\gamma_{k\rho} , \quad \text{(B7)}$$

the dielectric-constant impulse-response function becomes

$$G^{\epsilon\epsilon}_{cccc}(\mathbf{k},t) = \frac{f_\rho(k)}{\Omega_{k\rho}} \exp(-\gamma_{k\rho}t)\sin[\Omega_{k\rho}t + \varphi_\rho(k)] . \quad \text{(B8)}$$

Figures 7(a) and 7(b) illustrate the polariton-response-function amplitude $[f_{\rho=1}(k)]$ and phase $[\varphi_{\rho=1}(k)]$ dependence on wave vector and relative strength of the Raman (a) and the electro-optic (b) tensors, based on Eqs. (B6) and (B8). Values used for the phonon parameters are obtained from the fit of the $T = 10$ K experimental curve, where $\Omega_p = 771$ cm^{-1}, $\omega_{\rm TO} = 82$ cm^{-1}, and $\gamma_{\rm TO} = 13$ cm^{-1} [i.e., $\Sigma^R(\mathbf{k},\omega) = 0$, $\Sigma^I(\mathbf{k},\omega) = \gamma_{\rm TO}$]. These results are similar to those derived in the limiting cases $a \neq 0, b = 0$ and $a = 0, b \neq 0$ by Dougherty *et al.*[5] For $b = 0$, the impulsive-stimulated scattering amplitude increases monotonically with k while the phase is approximately zero. For $|b| \neq 0$ the amplitude shows a strong maximum at low wave vector (here around $ck/n \simeq 500$ cm^{-1}), and for $b > 0$, there is a value of ck/n where $f_1(k) \simeq 0$. This results from the cancellation of the scattering contribution from the Raman tensor by the electro-optic tensor, as discussed by Benson and Mills.[44]

From this appendix and Dougherty *et al.*,[5] the electro-optic and Raman tensors are only two different ways in which the radiation field couples to the polariton mode. This is in disagreement with Ref. 8 where it is claimed that the electro-optic and the Raman tensors contribute separately to $\chi^{(2)}$ and $\chi^{(3)}$. The relative contributions of these two tensors affect only the polariton amplitude and phase-response-function wave-vector dependence. The polariton-response-function time evolution is related to the intrinsic polariton-mode characteristics through the propagator poles and does not depend on the relative strength of the electro-optic and the Raman tensor, through which the polariton mode is generated and probed.

[1] D. P. Kien, J. C. Loulergue, and J. Etchepare, Opt. Commun. **101**, 53 (1993).
[2] D. P. Kien, J. C. Loulergue, and J. Etchepare, Phys. Rev. B **47**, 11027 (1993).
[3] P. Grenier, D. Houde, S. Jandl, and L. A. Boatner, Phys. Rev. B **47**, 1 (1993).
[4] H. J. Bakker, S. Hunsche, and H. Kurz, Phys. Rev. B **48**, 13524 (1993).
[5] T. P. Dougherty, G. P. Wiederrecht, and K. A. Nelson, J. Opt. Soc. Am. B **9**, 2179 (1992).
[6] T. P. Dougherty, G. P. Wiederrecht, K. A. Nelson, M. H. Garrett, H. P. Jensen, and C. Warde, Science **258**, 770 (1992).
[7] T. P. Dougherty, G. P. Wiederrecht, and K. A. Nelson, Ferroelectrics **120**, 79 (1991).
[8] P. C. M. Planken, L. D. Noordam, J. T. M. Kennis, and A. Lagendijk, Phys. Rev. B **45**, 7106 (1992).
[9] J. Etchepare, G. Grillon, A. Antonetti, J. C. Loulergue, M. D. Fontana, and G. E. Kugel, Phys. Rev. B **41**, 12362 (1990).
[10] A. D. Bruce and R. A. Cowley, Adv. Phys. **29**, 1 (1980).
[11] B. E. Vugmeister and M. D. Glinchuk, Rev. Mod. Phys. **62**, 993 (1990).
[12] G. E. Kugel and M. D. Fontana, Ferroelectrics **120**, 89 (1991).
[13] M. D. Fontana, E. Bouziane, and G. E. Kugel, J. Phys. Condens. Matter **2**, 8681 (1990).
[14] M. D. Fontana, A. Ridah, G. E. Kugel, and C. Carabatos-Nedelec, J. Phys. C **21**, 5853 (1988).
[15] E. Lee, L. L. Chase, and L. A. Boatner, Phys. Rev. B **31**, 1438 (1985).
[16] Y.-X. Yan and K. A. Nelson, J. Chem. Phys. **87**, 6240 (1987).
[17] Y.-X. Yan and K. A. Nelson, J. Chem. Phys. **87**, 6257 (1987).
[18] G. D. Mahan, *Many-Particle Physics* (Plenum Press, New York, 1982).
[19] R. A. Cowley, Adv. Phys. **12**, 421 (1963).
[20] I. Thomazeau, J. Etchepare, G. Grillon, G. Hamoniaux, and A. Orszag, Opt. Commun. **55**, 442 (1985).
[21] P. Grenier, D. Houde, S. Jandl, and L. A. Boatner, Can. J. Phys. **72**, 40 (1993).
[22] S. Ushioda and J. D. McMullen, Solid State Commun. **11**, 299 (1972).
[23] S. Ushioda, J. D. McMullen, and M. J. Delaney, Phys. Rev. B **8**, 4634 (1973).
[24] F. Vallée and C. Flytzanis, Phys. Rev. B **46**, 13799 (1992).
[25] M. D. Fontana, G. E. Kugel, L. Foussadier, W. Kress, and D. Rytz, Europhys. Lett. **23**, 427 (1993).
[26] C. H. Perry, R. Currat, H. Buhay, R. M. Migoni, W. G. Stirling, and J. D. Axe, Phys. Rev. B **39**, 8666 (1989).
[27] C. M. Foster, Z. Li, M. Grimsditch, S.-K. Chan, and D. J. Lam, Phys. Rev. B **48**, 10160 (1993).
[28] A. S. Barker, Jr., Phys. Rev. **165**, 917 (1968).
[29] A. S. Barker, Jr. and J. J. Hopfield, Phys. Rev. **135**, A1732 (1964).

[30]A. F. Penna, A. Chaves, and S. P. S. Porto, Solid State Commun. **19**, 491 (1976).
[31]C. Mavroyannis and K. N. Pathak, Phys. Rev. **182**, 872 (1969).
[32]C. Mavroyannis, Phys. Rev. B **3**, 2750 (1971).
[33]H. Uwe, K. B. Lyons, H. L. Carter, and P. A. Fleury, Phys. Rev. B **33**, 6436 (1986).
[34]H. Vogt, J. Phys. Condens. Matter **3**, 3697 (1991).
[35]P. Grenier, S. Jandl, M. Blouin, and L. A. Boatner, Ferroelectrics **137**, 105 (1992).
[36]J. Toulouse, X. M. Wang, L. A. Knauss, and L. A. Boatner, Phys. Rev. B **43**, 8297 (1991).
[37]J. Toulouse, P. DiAntonio, B. E. Vugmeister, X. M. Wang, and L. A. Knauss, Phys. Rev. Lett. **68**, 232 (1992).
[38]R. L. Prater, L. L. Chase, and L. A. Boatner, Phys. Rev. B **23**, 221 (1981).
[39]R. Migoni, H. Bilz, and D. Bäuerle, Phys. Rev. Lett. **37**, 1155 (1976).
[40]G. E. Kugel, M. D. Fontana, and W. Kress, Phys. Rev. B **35**, 813 (1987).
[41]G. E. Kugel, H. Mesli, M. D. Fontana, and D. Rytz, Phys. Rev. B **37**, 5619 (1988).
[42]B. E. Vugmeister and T. V. Antimirova, Phys. Status Solidi B **157**, 183 (1990).
[43]B. E. Vugmeister, Ferroelectrics **120**, 133 (1991).
[44]H. J. Benson and D. L. Mills, Phys. Rev. B **1**, 4835 (1970).
[45]N. N. Bogoliubov, *Lectures on Quantum Statistics* (Gordon and Breach, New York, 1967), Vol. 1, p. 213.
[46]J. J. Hopfield, Phys. Rev. **112**, 1555 (1958).
[47]A. H. Opie, Phys. Rev. **187**, 1168 (1969).
[48]D. L. Mills and E. Burstein, Rep. Prog. Phys. **37**, 817 (1974).
[49]R. S. Tripathi and K. N. Pathak, Nuovo Cimento B **21**, 289 (1974).